Observations and Impacts of the 10 September 2017 Solar Events at Mars: An Overview and Synthesis of the Initial Results

C. O. Lee[1], B. M. Jakosky[2], J. G. Luhmann[1], D. A. Brain[2], M. L. Mays[3], D. M. Hassler[4], M. Holmstrom[5], D. E. Larson[1], D. L. Mitchell[1], C. Mazelle[6], and J. S. Halekas[7]

C. O. Lee, clee@ssl.berkeley.edu

[1]Space Sciences Laboratory, University of California, Berkeley, CA 94720, USA.

[2]Laboratory for Atmospheric and Space Physics, University of Colorado, Boulder, Colorado, USA.

[3]CCMC/NASA Goddard Space Flight Center, Greenbelt, MD 20771, USA.

[4]Space Science and Engineering Division, Southwest Research Institute, Boulder, CO, USA.

This article has been accepted for publication and undergone full peer review but has not been through the copyediting, typesetting, pagination and proofreading process, which may lead to differences between this version and the Version of Record. Please cite this article as doi: 10.1029/2018GL079162

On 10 September 2017 late in the declining phase of Solar Cycle 24, some of the strongest solar activity of the solar cycle occurred in association with active region 12673 (AR2673), including an X-class solar flare and a fast coronal mass ejection (CME). Although AR2673 was not centrally facing Mars (~67° east in heliolongitude from the Sun-Mars line), the solar events impacted the local space weather environment at Mars. We give an overview of the observations at Mars obtained from various missions, including Mars Atmosphere and Volatile Evolution (MAVEN), Mars Science Laboratory (MSL), and Mars Express (MEX). Numerical results from the Wang-Sheeley-Arge (WSA)-Enlil-cone model system together with observations at Earth/L1 and STEREO-A are also presented to provide a more global heliospheric context of the event period. We discuss some of the initial results on the space weather impacts at Mars, which include heating of the upper atmosphere by solar

[5]Swedish Institute of Space Physics,
Kiruna, Sweden

[6]Institut de Recherche en Astrophysqiue
et Plantologie, Universit de Toulouse,
CNRS, UPS, CNES, Toulouse, France.

[7]Department of Physics and Astronomy,
University of Iowa, Iowa City, IA 52242,
USA.

flare emissions, flare-related enhancements of ion and neutral densities, high fluxes of solar energetic particles impacting the atmosphere and the surface, bright emissions of a diffuse (global) aurora, deeply penetrating interplanetary magnetic fields over the Martian dayside due to the CME impact, and enhanced atmospheric escape rates.

Keypoints:

- An X8.2 solar flare, ICME, and associated solar energetic particles impacted Mars beginning on 10 September 2017.
- This was the largest event observed at Mars simultaneously in orbit by the current flotilla of spacecraft and at the surface by a lander.
- Observations included the solar event, significant effects on the upper atmosphere and ionosphere, and influence on escape of gas to space.

1. Introduction

When an X8.2 class flare and a fast and wide coronal mass ejection (CME) erupted from active region 12673 (hereafter, AR2673) on 10 September 2017, the space weather impact was widespread and observed at multiple locations including Earth, Mars, and STEREO-A (hereafter, STA) [*Kaiser*, 2005]. The collection of papers in this GRL volume focuses on the observations and impacts at Mars triggered by these solar eruptive events. The space weather effects at Mars were simultaneously observed by instruments across several Mars missions, including Mars Atmosphere and Volatile Evolution (MAVEN), Mars Science Laboratory (MSL), Mars Express (MEX), Mars Odyssey (MO) and also Trace Gas Orbiter (TGO). A collection of papers that discusses the observations and impacts at Earth may be found in the Space Weather Journal (2018).

These September events began with two large M-class flares and one X-class flare observed at Mars [*Chamberlin et al.*, 2018] together with CME activity seen in the solar coronagraphs at Earth and STA. High fluxes of solar energetic particles (SEPs) associated with the flare and CME eruption were also detected (e.g., see *Luhmann et al.* [2018]). In Section 2 we provide an overview of the solar and heliospheric observations of the 10 September 2017 solar activity to provide context for Sections 3– 6 where we present and synthesize the initial results presented in this GRL volume on the space weather impacts at Mars. Numerical results for the event period[1] from the Wang-Sheeley-Arge (WSA)-Enlil coupled solar corona-solar wind model (hereafter, WSA-Enlil) [*Arge et al.*, 2004; *Odstrcil*, 2003]) are used to illustrate the global context of the solar and heliospheric sources of the space weather conditions observed at Mars during this event period.

2. Solar Eruptive Activity on 10 September 2017

The strong solar activity began with the eruption of the X8.2 class flare from AR2673 on 10 Sept 2017. The flare was initially observed at Earth by the NOAA Geostationary Operational Environmental Satellites (GOES, [*Aschwanden*, 1994]) X-ray flux instrument in the 0.1–0.8 nm channel for solar soft X-rays. The event start time was ∼15:35 UT and peaked at ∼16:06 UT before slowly returning to the background levels at ∼16:31 UT.[2] Solar images taken near Earth from the Solar Dynamics Observatory (SDO) Atmospheric Imaging Assembly (AIA) [*Lemen et al.*, 2012], such as Figure 1a (top panel), show that AR2673 was located around the western limb of the solar disk (∼W90°, where 0° longitude is located at the center of the solar disk) when the flare erupted. At the STA location, AR2673 was seen near the eastern limb (∼E90°), as shown in Figure 1b (top panel) from the STA Extreme Ultraviolet Imager (EUVI).

Although there is no solar imager present at Mars, the Extreme Ultraviolet Monitor (EUVM; *Eparvier et al.* [2015]) on board MAVEN did observe an increase in solar irradiance during the flare (*Chamberlin et al.* [2018]). Located ∼0.66 AU further away, EUVM detected the flare ∼5.5 minutes after GOES. From the Mars vantage point, AR2673 would have been visible on the solar disk at ∼E67°. The inset of Figure 1c illustrates the relative locations of Earth, Mars, and STA with respect to the solar longitude location of AR2673 during the event period. MAVEN/EUVM can measure the solar emissions from the hot solar corona in the wavelength range of 0.1–7 nm (science channel B, hereafter EUVM-B), which responds to solar flares in a manner similar to the GOES X-ray flux instrument. MAVEN/EUVM also measures the hydrogen Lyman-α emission at 121.6 nm

(science channel C), which responds to the increase in solar EUV and the more impulsive (earlier) phase of the solar flare. Figure 3a, which will be discussed in detail in Section 3, shows EUVM-B soft X-ray irradiance observations of the X-class flare with a peak flare time at 15:40:30 UT (dashed magenta line labeled 'F'). Also, the MAVEN/SEP instrument [*Larson et al.*, 2015] detected the solar flare hard x-rays in its 'thick' detector at ∼15:54 UT, with a similar peak time of 16:02 UT as the Lyman-α emission (not shown).

The solar activity around AR2673 continued with the eruption of a fast and wide CME. The SDO/AIA 211 image taken at 15:54:35 UT shows a bright CME magnetic field loop around AR2673 (Figure 1a, top panel). The CME was later observed by the Solar and Heliospheric Observatory (SOHO) Large Angle and Spectrometric Coronagraph (LASCO; *Brueckner et al.* [1995]) and the STA Sun Earth Connection Coronal and Heliospheric Investigation (SECCHI) COR2 coronagraph. The leading edge of the CME entered the LASCO/C2 FOV (1.5–6 $R_\odot$) at 16:00 UT and the LASCO/C3 FOV (3.8–32 $R_\odot$) between 16:06 UT to 16:18 UT. Based on these observations, an initial linear speed of ∼3300 km s^{-1} was estimated[3]. The bottom panels of Figure 1a and 1b show a bright and wide CME from the vantage points of Earth (LASCO/C3) and STA (SECCHI/COR2), respectively.

High-energy SEP protons associated with this fast CME were observed at Earth and STA as well as at Mars. Figure 1c (top to bottom) shows the SEP proton measurements by GOES-13, MAVEN/SEP, and the STA High Energy Telescope (HET; *von Rosenvinge et al.* [2008]). Because of the western location of AR2673 with respect to the Sun-Earth line, GOES-13 detected the prompt arrival of SEP protons (at ∼16:30 UT on 10 Sept 2017 for the 165 MeV energy channel shown) due to the apparent magnetic field line

connection of Earth to the CME-driven shock source near the Sun. Meanwhile, AR2673 was located at E67° with respect to the Sun-Mars line and thus MAVEN/SEP detected a later arrival of SEP protons (at ∼22:00 UT on 10 Sept 2017 for the 80–220 MeV energy channel shown) when the CME shock was further away from the Sun and magnetically connected to Mars e.g., see Figure 6c in *Luhmann et al.* [2018]. STA/HET detected SEP protons even later (at ∼06:00 UT on 11 Sept 2017 for the 60–100 MeV energy channel shown) when the CME shock had travelled further outward to magnetically connect with STA e.g., see Figure 6b in *Luhmann et al.* [2018].

The WSA-Enlil simulation snapshots (Figure 2) show the evolution of the ecliptic solar wind speeds and CME structure over a period of several days. Panels 2a– 2b show the parameterized CME clouds for two slower CMEs that erupted on 9 Sept 2018 and merged together (CME1+2) and the faster CME that erupted on 10 Sept 2017 (CME3). Since CME3 is moving faster and propagating in the same radial direction as CME1+2, CME3 interacts with CME1+2 from behind to become a single, merged CME structure (panel 2c), as described by *Guo et al.* [2018b]. Panels 2d– 2f show the modeling results of the merged CME structure encountering Venus and STEREO-B before reaching Mars at ∼00:00 UT on 13 Sept 2017, ∼60 hours after the CME eruption. In Section 5 we will show that the modeled arrival time of the CME at Mars matches well with the in situ observations of the event.

For this article, we use the WSA-Enlil simulation results as a tool toward interpreting the solar wind and CME observations at Mars. The simulation details are described in the Space Weather paper by *Luhmann et al.* [2018] that uses the Enlil results to model the

associated SEP observations for the July and September 2017 event periods. In general, the limitations of WSA-Enlil to accurately model the CME event include the uncertainties in the input solar photospheric field maps to drive the background solar wind simulations, the use of a geometrical cone shape to approximate the shape of a CME, the accuracy of the CME parameterization (injection direction, time, and size), and the lack of the ejecta field description in Enlil, which affects the CME expansion during the propagation [**??***Mays et al.* [2015]]. Nevertheless it is found that the simulation often produces a good first-order approximation to the heliospheric conditions associated with real CMEs, including time series of plasma velocities and ICME shock arrival times.

3. Heating of Mars' Atmosphere by the Flare Photons

The X8.2 class flare on 10 Sept 2017 was the largest known event of Solar Cycle 24 to impact Mars and the largest event observed to date by MAVEN/EUVM. While previous studies have reported the Mars ionosphere [*Gurnett et al.*, 2005] and thermosphere [*Thiemann et al.*, 2015] responses to solar flares for individual events using separate spacecraft observations, multiple instruments onboard MAVEN simultaneously observed both the thermosphere and ionosphere response to the 10 Sept 2017 flare. Although the bulk ionospheric plasma enhancement is expected to be brief, following the time profile of the flare [*Mendillo et al.*, 1974; *Lollo et al.*, 2012], the thermosphere is seen to respond more slowly.

At ∼170 km in the thermosphere, *Jain et al.* [2018] report a temperature increase of ∼70 K during the flare, based on airglow measurements from the MAVEN Imaging UltraViolet Spectrograph (IUVS) instrument. They also found that the flare heating was more pronounced at the low-to-mid latitudes of Mars. One possible explanation is that

upper atmosphere dynamics prevented the heating from the flare near the subsolar point to dissipate to higher latitudes. An example of the MAVEN/IUVS temperature time profile is shown in Figure 3k to illustrate the timing of the thermospheric response with the solar irradiance enhancement (Figure 3a).

Elrod et al. [2018] investigated the flare emission response of the upper atmospheric neutral species (Ar, CO_2, CO, O and N_2) observed in situ by the MAVEN Neutral Gas and Ion Spectrometer (NGIMS) [*Mahaffy et al.*, 2015] and found that the atmosphere heated on a timescale similar to the duration of the flare event. Specifically, they found that during one orbit of observations coincident with the flare event, there was a significant density and temperature enhancement in the Martian neutral exosphere above 195 km. By the following orbit ($\sim$4.5 hours later), the observed densities and temperatures were at the approximate pre-flare event values. An example of the Ar densities (color contours) for a given altitude is shown in Figure 3l. A comparison with the MAVEN/EUVM observations (Figure 3a) and IUVS thermospheric temperature (Figure 3k) shows that enhanced Ar densities are correlated with the increase of solar irradiance. Since Ar is an inert gas, changes in the Ar temperatures are a good indicator of temperature changes in the upper atmosphere. *Elrod et al.* [2018] showed that the Ar density at a fixed altitude of 225 km increased by a factor of $\sim$4, and that the Ar temperature increased by $\sim$90 K during the peak of the flare event. For all neutral species observed by NGIMS, the temperatures increased by $\sim$100 K.

The first in-situ observed flare response of the topside ionosphere thermal plasma temperature and composition is reported by *Thiemann et al.* [2018]. Using observations from

MAVEN/EUVM, NGIMS, and the Langmuir Probe and Waves (LPW) [Andersson et al., 2015] together with model calculations, they found that photon energy deposition was enhanced by ∼80% at 110 km in the thermosphere, where most of the soft X-ray (SXR, 0.1-10 nm) photons deposited their energy, and the total photoionization rate increased by 500% at these altitudes. In the upper atmosphere, the total ionization rate increased by 20%. With the presence of more neutrals at high altitudes (due to an expanded neutral atmosphere), the MAVEN observations showed that the electron densities (n_e) and ion densities (for O_2^+, CO_2^+, O^+) increased (see Figures 2 and 3 in *Thiemann et al.* [2018]) while the electron heating was suppressed below ∼220 km due to efficient electron cooling by CO_2. Generally speaking, the observed changes in the ionosphere during the MAVEN observations obtained after the time of the flare peak are due to the expansion of the neutral atmosphere and altered neutral composition. In terms of compositional changes in the ionosphere, *Thiemann et al.* [2018] reported an increase in the production of O and thus an increase in the relative abundance of O at a fixed pressure, which has implications for photochemical escape (Section 6).

Xu et al. [2018b] investigated the low-altitude ionospheric response to the X8.2 flare by SuperThermal Electron Transport (STET) model to simulate the photoelectron spectra and ion production rates and densities for periods before the flare, during the flare peak, and during the first MAVEN in-situ observations of the period after the flare peak. A good agreement was found between the modeled photoelectron spectra and observations. In addition, the carbon Auger peak in the photoelectron spectra, produced by SXR photons ionizing the inner shell electrons and the sequential relaxation of electronically excited

carbon ions by emitting electrons with a fixed energy ∼250 eV, was repeatedly identified in the Martian ionosphere for the first time, due to the higher photoelectron fluxes during the flare interval. Based on their modeled O_2^+ and CO_2^+ densities for the three event intervals, they found that the enhancements due to the flare at a fixed altitude increased by a few tens of percent up to ∼1500%.

Global upper atmospheric modeling of the flare event and comparison with the MAVEN in situ observations of the atmospheric response are reported by *Fang et al.* [2018]. The MAVEN/LPW, NGIMS, and IUVS measurements are routinely made below ∼ 500 km altitude along ∼40-minute periapsis segments of the ∼4.5-hour orbit. During the flare event, the nearest time that these instruments made measurements occurred at 17:35 UT on 10 Sept 2017, ∼1 hour after the flare peak time (16:24 UT, based on 0–91 nm irradiance by *Thiemann et al.* [2018]). Moreover, the NGIMS ion densities (e.g., for O_2^+, CO_2^+, O^+) were only measured during alternate orbits. Considering the limited spatial and temporal coverage of MAVEN, the modeling study of *Fang et al.* [2018] provides important context to understand the solar flare impact on a global scale and its evolution with time. The modeling work represents the first numerical attempt to quantify global perturbations of the Martian upper atmosphere in response to a solar flare event using realistic flare irradiance. They found that the atmospheric perturbations enhanced with increasing altitude and reached the maximum level ∼1.5 hours after the peak of the flare, and that the neutral atmosphere took >10 hours to recover from the flare-induced perturbations before returning to its pre-event level.

4. SEPs at Mars

While the Martian atmosphere was responding to the energetic input from the X8.2 flare, a fast and wide CME had erupted in the general vicinity of the flare site. As the shock and the driver CME propagated toward and magnetically connected with Mars (e.g., Figure 2c– 3f), the highest energy SEPs were detected by several instruments from MAVEN, MEX and MSL Radiation Assessment Detector (RAD).

4.1. SEPs in Near-Mars Space

As discussed in Section 2, MAVEN/SEP detected 15–100 MeV and 80–220 MeV SEP protons several hours after the CME eruption. These high energy SEPs penetrated through the MAVEN/SEP stack of silicon detectors called 'foil', 'thick', and 'open' to trigger a Foil-Thick-Open (FTO) event type (see Figure 6 and related discussion in *Larson et al.* [2015]). The direct measurements of incident energies and fluxes for SEPs detected in the FTO bins are currently unavailable since the instrument is optimized to measure 20 keV–6 MeV protons (energies that are important for atmospheric escape). For the FTO observations reported here, the detected energy information together with the MAVEN/SEP instrument response matrices are used to constrain the incident energy range. Figure 3c shows the 15–100 MeV and 80–220 MeV SEP protons, with the vertical blue line ('E') marking the SEP proton arrival time to Mars (∼22:00 UT on 10 Sept 2017). The peak detection of 80–220 MeV SEP protons occurred at ∼18:53 UT on 11 Sept 2017 while peak detection for 15–100 MeV SEP protons occurred at ∼17:58 UT on 12 Sept 2017.

A sharp rise was observed in the MAVEN energetic particle observations due to the ICME shock arrival at ∼02:52 UT on 13 Sept 2012. This peak can be seen most clearly

in the MAVEN Solar Wind Electron Analyzer (SWEA) penetrating counts in Figure 3b (vertical black line, 'S'). The source for penetrating counts in SWEA are SEP protons with energies of a few tens of MeV (e.g. Figure 3c, cyan time series) and SEP electrons with energies of a few MeV penetrating the instrument housing. MAVEN/SEP also detected a sharp peak in the measured fluxes for 20 keV–6 MeV SEP ions and 20 keV–200 keV SEP electrons, as indicated by the darkest red color shown in Figure 3d and 3e. Such a peak in the particle observations is consistent with an energetic storm particle (ESP) enhancement that occurs when an ICME shock passes the observer. Consistent with these observations, WSA-Enlil modeled the ICME impact to occur at Mars shortly after 00:00 UT on 13 Sept 2017 (Figure 2f). After the shock arrival the energetic particle enhancements slowly declined.

Penetrating background counts were also measured by the MEX/ASPERA-3 IMA instrument [*Futaana et al.*, 2008; *Capalbo*, 2010], as shown in Figure 3b. The overall trend follows observations from MAVEN/SWEA and also MAVEN/SEP-FTO (Figure 3c). *Ramstad et al.* [2018] reported the first attempt to calibrate the IMA penetrating background counts with the MAVEN/SEP-FTO data. In doing so, they found that the IMA background counts are due to >1 MeV SEP electrons and >20 MeV protons. Given the high flux of SEPs measured by MAVEN/SEP during this event, they compared the counts for this event period to those over the entire MEX mission to date since 2004 and found that the September 2017 SEP event was the 4th strongest event detected at Mars since 2004.

4.2. SEPs in the Martian Upper Atmosphere

Harada et al. [2018] investigated the ionosphere response to SEPs using the nightside ionosphere observations from the MEX Mars Advanced Radar for Subsurface and Ionosphere Sounding (MARSIS) instrument [*Gurnett et al.*, 2008] together with the MAVEN dayside observations. The MARSIS instrument in particular has been making ionospheric sounding measurements of the Martian topside ionosphere, which can be used to infer the vertical electron density profiles of the topside ionosphere. During the SEP event period, MARSIS detected ionospheric echoes with unusually high peak electron densities (∼1–2×10^4 cm^{-3}) at ∼120 km altitudes in the deep nightside ionosphere, suggesting enhanced impact ionization by precipitating energetic particles (e.g., *Withers* [2011]; **?**]; *Guo et al.* [2018a]). Associated with high SEP fluxes, MARSIS also observed the disappearance of ground reflection due to radio wave attenuation (i.e., radio blackout periods) by enhanced ionization below the peak density altitude of ∼100–150 km [*Fowler et al.*, 2015; *Girazian et al.*, 2017].

During the period of high SEP activity, SEPs penetrated deep into the atmosphere to produce a bright diffuse aurora caused by global precipitation of energetic particles [*Schneider et al.*, 2018]. The diffuse aurora was captured in spectral images taken in the mid-UV range (195-220 nm) by MAVEN/IUVS during multiple apoapse orbit segments on 13 Sept 2017. By mapping the spectral images onto a Mars geographic coordinate system, *Schneider et al.* [2018] constructed the first complete image of the diffuse aurora at Mars showing a fairly uniform emission enhancement across the observable nightside disk. Compared to the diffuse aurora event reported previously [*Jakosky et al.*, 2015b],

the emission from this event was 25 times brighter. Based on the IUVS limb scans, these emissions originated from ∼70 km altitude.

In the first report of a diffuse aurora, *Schneider et al.* [2015] found a correlation between the auroral emission and SEP electron events. The peak brightness observed at ∼60–70 km suggested an association with 100 keV SEP electrons penetrating down to this altitude range in the Martian atmosphere to excite auroral emission. For the September 2017 event, Figure 3e shows the IUVS auroral emission (black circles) overplotted with the 20–200 keV SEP electron fluxes. It can be seen that there is no clear distinction for a SEP electron or proton source of this auroral emission [*Schneider et al.*, 2018].

In addition to the observation of a diffuse aurora associated with the SEP activity, *Schneider et al.* [2018] also reported the detection of discrete auroral emission features that occurred for a short interval on 14 Sept 2017. From a sequence of IUVS spectral image swaths mapped onto the Mars geographic coordinate system, *Schneider et al.* [2018] constructed an image of the discrete aurora over the visible nightside disk, which showed the emissions appearing as bright localized patches and curved 'wisp' shapes. Overplotting these features onto a statistical map of open and closed magnetic field line topology, they found that the discrete auroral emission features occurred in or near regions with high probability of open magnetic field topology. However, it is currently unclear whether the source of these emissions are due to low-energy electrons accelerated locally in crustal fields, or due to the focusing of high-energy SEPs by the crustal magnetic fields [*Schneider et al.*, 2018]. The occurrence of the discrete aurora during the declining phase of SEP event period (see their Fig. 3) is consistent with the correlation previously reported by

Brain et al. [2006], that the local conditions favorable for discrete aurora to occur are during the time when the plasma environment as a whole is already disturbed.

4.3. SEPs at the Martian Surface

With no global magnetic field at Mars to deflect the charged particles nor a thick atmosphere to shield against them, SEPs with energies of 150 MeV/nuc and higher can penetrate down to the surface [*Hassler et al.*, 2014; *Guo et al.*, 2018a]. The detection of such an event at Mars is analogous to the ground-level enhancement (GLE) event that occurs at Earth when ground-based instruments detect secondary neutrons caused by high energy protons impacting the top of Earth's atmosphere. Typically, a GLE event is caused by SEPs that are accelerated by a strong CME shock formed close to the Sun and is observed when Earth is magnetically connected to it at ∼W90°. On 10 Sept 2017, a GLE event was observed at ∼16:15 UT at Earth, caused by ∼2 GeV protons impacting the terrestrial atmosphere [*Guo et al.*, 2018b].

At Mars a GLE event was also observed. As reported by *Zeitlin et al.* [2018], *Ehresmann et al.* [2018], and *Guo et al.* [2018b], MSL/RAD observed enhancements in the surface radiation dose rates and particles fluxes beginning at 19:50 UT on 10 Sept 2017, making this event the first simultaneous GLE observation at two planets. Located at the Gale Crater, MSL/RAD has been continuously measuring the radiation environment at the surface since 2012 [*Hassler et al.*, 2014]. The source of the radiation is predominantly galactic cosmic rays (GCRs) and occasionally SEPs penetrating down to the surface. During the SEP event, RAD detected an increase above the GCR-induced background levels in the surface proton environment by factors up to 30 for <100 MeV protons and

factors up to 4 for >135 MeV protons, in addition to the increase in the surface ^{4}He flux (below 100 MeV nuc^{-1}) by a factor of 10 [*Ehresmann et al.*, 2018]. Considering that protons lose roughly 150 MeV of energy passing through the Martian atmosphere, the detection of $< \sim$100 MeV SEP protons at the surface by MSL/RAD is consistent with observations of the 80-220 MeV protons by MAVEN/SEP in orbit (i.e. Figure 3c).

For the surface dose rates, MSL/RAD observed factors of 2–3 increase above the GCR-induced background levels [*Zeitlin et al.*, 2018]. In terms of the radiation hazards posed by SEPs, the integrated dose over a 30-day interval including the SEP period was well below the NASA exposure limits for astronauts [*Zeitlin et al.*, 2018]. Figure 3m shows the measured dose rates from the MSL/RAD-E (plastic) detector. As described by *Zeitlin et al.* [2018], for SEPs to go through the atmosphere and deposit energy onto MSL/RAD-E, SEP ions with incident energy of at least 275 MeV nuc^{-1} are required. Thus, SEP protons at these energies travel faster such that the rise and peak of the MSL/RAD-E dose rate enhancements is seen to occur earlier than rise and peak of the MAVEN/SEP-FTO 80–220 MeV proton measurements shown in Figure 3c.

5. Response of Mars to the ICME Impact

The solar wind have been continuously monitored by MEX since 2004 [*Ramstad et al.*, 2015] and MAVEN since 2014 [*Halekas et al.*, 2017; **?**]. Panels 3f– 3i show the values observed away from the Martian bow shock and averaged over an orbit for the solar wind speed, density, dynamic pressure and total magnetic field during 9 Sept to 18 Sept 2017 by MEX (blue filled circles) and MAVEN (red filled circles). The MAVEN solar wind parameters were derived from the Solar Wind Ion Analyzer (SWIA) [*Halekas et al.*,

2015] and Magnetometer (MAG) [*Connerney et al.*, 2015] measurements based on the methodology described in Section 3 of *Halekas et al.* [2017]. Figure 4 illustrates the MEX and MAVEN orbit tracks, which are color coded light to dark to represent time (earlier to later). The MEX apoapsis segment was positioned well upstream to measure the solar wind. Meanwhile, as the MAVEN orbit precessed its apoapsis location approached near the dusk-dawn terminator within the nominal bow shock location (outer solid line in Figure 4a). Therefore, MAVEN was only occasionally exposed to the solar wind. To provide a more complete MAVEN data set, included in panels 3f– 3g are the solar wind speeds and densities estimated from the SWIA penetrating proton measurements made over an altitude range of 150–250 km (see Section 3.2 in *Halekas et al.* [2017]). The proxy data (red open squares) is merged with the upstream measurements (filled circles) to a common two-hour grid using a simple nearest-neighbor interpolation.

Prior to the solar eruptive activity, both missions were measuring relatively quiet conditions, where the solar wind speed was below 400 km s^{-1} and dynamic pressure at 1 nPa. The conditions were moderately disturbed starting on 10 Sept 2017, when fluctuations in the solar wind densities were observed including the passage of a moderately fast solar wind stream and the related stream interaction region (SIR). The source of this stream is likely the low-to-mid-latitude coronal hole imaged by STA/EUVI in Figure 1b. Starting at 23:30 UT on 10 Sept 2017 (after the vertical blue line, 'E'), the solar wind density, dynamic pressure and interplanetary magnetic field (IMF) magnitude were higher (8 cm^{-3}, 2 nPa, 13 nT; the peak values were likely higher but not observed) followed by an increase in the solar wind speed ($\sim$530 km s^{-1}).

During the ICME event interval, the observation coverage above the bow shock was limited for MEX due to power restrictions. Meanwhile, MAVEN was located within the nominal bow shock location and thus only the penetrating proton proxy estimates for the solar wind density and speed were available. Thus for additional context, the model results from WSA-Enlil are also plotted in panels 3f–3i (black line). The modeled ICME arrived at ∼4:00 UT on 13 Sept 2017, with peaks in the modeled speed, density, dynamic pressure, and total IMF (820 km s^{-1}, 3.2 cc^{-1}, 3.4 nPa, 3.8 nT). The overall consistency of the modeled shock arrival time and peak values with the observations gives us confidence in using the WSA-Enlil simulation results together with observations for determining the ICME impact scenario at Mars. From Figure 2f, it is suggested that the ICME made a direct impact at Mars as oppose to a glancing blow, as was the case for Earth. This scenario is also suggested by observations. In panels 3b– 3c, a brief drop-out is seen in the penetrating particle and SEP observations during the ICME interval. This feature, highlighted in gray, appears most prominently in the MAVEN/SWEA observations (panel 3b) and MAVEN/SEP-FTO observations (panel 3c). Such a 'bite-out' is likely caused by the passage of the ICME magnetic cloud, suggesting that Mars intersected the ICME structure more centrally (Figure 2f).

A >20% decrease in the surface radiation dose rates was measured by MSL/RAD during the ICME event [*Guo et al.*, 2018b]. Figure 3m shows that the onset of the decrease began at ∼2:52 UT on 13 Sept 2017, during the time of the observed ICME shock impact (black vertical line, 'S') and that the deepest decrease in dose rate occurred during the encounter of the ICME magnetic cloud with Mars (interval shaded in gray). The decrease in the dose

rate is due to the shock and/or ICME magnetic cloud acting as a magnetic barrier for the charged particles (e.g., GCRs) to reach the surface. Such an event at Mars is equivalent to the so-called Forbush decrease detected by neutron monitors at Earth [*Cane*, 2000]. Compared to the Forbush decrease events observed previously at Mars, (e.g., *Witasse et al.* [2017]; *Guo et al.* [2018a]), the 13 Sept 2017 event is the deepest one observed to date by MSL/RAD.

The response of the local magnetic topology to the ICME impact is investigated by *Xu et al.* [2018a], using MAVEN/SWEA and MAG together with MHD modeling results (e.g., *Ma et al.* [2018]). Understanding the changing magnetic topology (closed, open, or draped magnetic field configuration) driven by variable solar wind conditions has important implications for energetic particle precipitation patterns in the atmosphere and also for mechanisms that control low energy 'cold' ion escape (e.g. ion trapped by closed field lines, polar wind-like ionospheric outflow from below 160–200 km along open field lines connected to the solar wind, and ions stripped away by draped fields via the $j \times B$ force). Figure 3j shows the magnetic topology for draped, open and closed field lines (blue, green and red, respectively), where each vertical segment represents observations during a MAVEN orbit versus altitude.

The deepest draped field penetration was observed after the ICME shock arrival (blue vertical segment coinciding with the black vertical line marked 'S' in Figure 3j). With the enhanced dynamic pressure from the ICME encounter, the draped IMF penetrated down to 200 km into the Martian atmosphere over the northern hemisphere. From the MHD results, *Xu et al.* [2018a] also found that more open field lines occurred over the

southern hemisphere (see Figures 4b and 4d of *Xu et al.* [2018a]). These results suggest enhanced cold ion escape occurs at lower altitudes where the ion densities are higher [*Xu et al.*, 2018a]. This disturbed magnetospheric configuration lasted for about two days. In addition to the ICME interval, *Xu et al.* [2018a] also reported that during the SIR encounter (∼2:34 UT on 11 Sept 2017) the draped IMF extended down to an altitude of ∼300 km.

From *Harada et al.* [2018], the low altitude (< 1000 km) magnetic field magnitude that was directly measured by MAVEN and deduced by MEX/MARSIS showed a significant enhancement over a wide range of solar zenith angles (SZAs). This is presumably caused by the high solar wind dynamic pressure during the ICME encounter. From a comparison of these measurements with Mars Global Surveyor observations, *Harada et al.* [2018] suggested that the September 2017 ICME event can be classified as a very high dynamic pressure event but weaker than the Halloween 2003 event [*Crider et al.*, 2005].

6. Implications for atmospheric escape

The flare, CME, and SEP events reported here provide an opportunity to examine the impact on atmospheric escape. Modeling studies (e.g. *Harnett et al.* [2006]; *Ma et al.* [2007]; *Dong et al.* [2015]) have suggested that atmospheric escape rates increase during time periods of disturbed solar wind. Observational studies (e.g. *Futaana et al.* [2008]; *Edberg et al.* [2010]; *Jakosky et al.* [2015b]; *Ramstad et al.* [2017]) generally support this idea, though evaluating global escape rates during such periods is hampered in at least two ways. First, such events have sufficiently short duration that a spacecraft at a given location cannot sample all relevant escape channels from Mars. Second, increased fluxes

of SEPs can lead to increased instrument background levels. Disturbed time periods also provide a foothold for evaluating atmospheric escape at earlier epochs in Mars history, since the solar and solar wind inputs during such time periods are likely to have been more intense than the current quiescent conditions (e.g. *Ribas et al.* [2005]; *Wood et al.* [2005]).

Atmospheric escape at Mars (or any planet) proceeds through a variety of physical mechanisms, each of which results in providing upper atmospheric particles with sufficient energy to escape the planet. Measurements from MAVEN during the event, as well as models of the event time period, have enabled estimates of the change in escape rates for most of these processes.

The escape of hydrogen from Mars is dominated by thermal escape, and estimates of the rate of loss typically require knowledge of densities and temperatures in the exobase region. *Mayyasi et al.* [2018] used in situ measurements of CO_2 and Ar densities from MAVEN/NGIMS to constrain the neutral upper atmospheric temperatures and observations of hydrogen Lyman-α emission intensities by MAVEN/IUVS are fit to a spherically symmetric radiative transfer model for the upper atmosphere to derive the exobase density. This model was then used to estimate the hydrogen thermal escape rate. Driven by an increase in the exobase temperature of hydrogen, the escape rates increased by a factor of $\sim$5 during the event.

In regards to oxygen, these atoms are too massive to escape thermally from Mars in any significant amount, and instead escape largely by photochemical processes whereby molecular oxygen ions dissociatively recombine. The response of the Martian ionosphere to

the X8.2 flare was explored by *Thiemann et al.* [2018], who used MAVEN measurements of T_e, abundances of O_2^+ and atmospheric neutral densities to estimate photochemical escape rates using the model of *Lillis et al.* [2017]. They found a noticeable (∼50%) increase in oxygen escape during a single orbit (∼4.5 hr) following the flare. This increase in photochemical escape was also inferred from coupled global simulations by *Lee et al.* [2018] of the Martian exosphere, thermosphere, and plasma environment for time periods encompassing the flare. They found an increase of ∼20% in the escape rate shortly following the flare, and a rapid decrease within ∼2.5 hours followed by a gradual return to nominal escape conditions.

Measurements of planetary ion escape are continuously made by MAVEN and have been evaluated based on the fluxes of heavy ions measured in a spherical shell with thickness of 0.2 R_M and centered around Mars at 1.35 R_M (∼1200 km altitudes) [*Brain et al.*, 2015]. Figure 5 shows the comparison of the outward-directed planetary heavy ion fluxes measured between 10 Sept 2017 through 18 Sept 2017 with the median outward ion fluxes at similar SZAs recorded over many months. In general, the observed escaping fluxes during the event are lower than those typically recorded by MAVEN. However, there are a few brief time periods, particularly after the ICME arrival, where instantaneous escaping fluxes are enhanced by a factor of ∼40. Integrated over the entire event period from flare arrival until after the ICME passage, the average escaping flux is enhanced by a factor of ∼2. We further note that the limited MAVEN orbital coverage during the event prevents a true assessment of the global change in ion escape rates because other regions could have experienced different magnitudes of enhancement in escaping fluxes. We take these

results as indicating that escape fluxes increased in at least some locations, and may have increased globally.

A global picture of ion escape during the event period is, however, made possible using simulations validated by observations. The CME event was simulated by *Ma et al.* [2018] using an MHD model and by *Romanelli et al.* [2018] using a hybrid model. Both global plasma models were driven with MAVEN and proxy measurements of the solar EUV photon flux, solar wind, and IMF at Mars. *Ma et al.* [2018] used the MHD model to run both steady-state and time-dependent simulations, and showed increases in heavy ion escape of a factor of 10–20, with rates as high as $\sim 3 \times 10^{25}$ s^{-1} for at least $\sim$5 hours, in excess of those reported by *Lee et al.* [2018] for photochemical escape using the same model framework. Both models showed good agreement with quantities measured by MAVEN along its orbit, such as magnetic field strength and direction, plasma velocity, and plasma density. This agreement gives confidence to the ability of the models to estimate ion escape rates. *Romanelli et al.* [2018] ran the hybrid model for three steady-state cases corresponding to three different time periods encompassing the CME event. They found that the escape fluxes of O^+ were enhanced by a factor of 2.5 during the event – much less than the enhancement obtained from the MHD model. In addition, they found that the escape of H^+ (not simulated by the MHD model) increased by a factor of $\sim$10, to $\sim 2 \times 10^{26}$ s^{-1}. We note that this rate is roughly comparable to thermal escape rates for neutral hydrogen that were reported by *Mayyasi et al.* [2018].

7. Concluding Remarks

The 10 September 2017 solar eruptive event provided an opportunity for instruments on board MAVEN, MEX, and MSL, to simultaneously observe the space weather impact at Mars. The timeline of the events summarized in this overview is presented in Table 1. The response of Mars to the solar events included the heating of the atmosphere by an X-class flare, global auroral emissions due to particle precipitation related to the high influx of SEPs, dramatic changes in the surface radiation environment due to high energy SEP protons, deep penetration of magnetosheath fields upon the ICME impact, and indications of enhanced planetary ion escape.

While solar flares and CME eruptions occur throughout the solar cycle, such relatively rare strong events have not been previously observed in such detail at Mars. The availability of supporting observations from other heliospheric vantage points and contextual information from global solar corona-solar wind modeling results also increases the scientific value of this event. One other event that greatly impacted Mars and Earth was the well-known Halloween Storm of 2003 [*Crider et al.*, 2005; *Gopalswamy et al.*, 2005]. However, only limited observations were available for interpretation of the Mars response. In addition, the September 2017 event observations at Mars are particularly valuable for providing a different solar and heliospheric perspective of space weather consequences. For example, *Luhmann et al.* [2018] used MAVEN/SEP proton observations to establish the heliospheric scenario for the widespread SEP occurrence during the event period.

However, perhaps of most importance are the potential implications of these observations at Mars for what they may tell us about how a terrestrial planet other than Earth with its own distinctive characteristics of size, atmosphere, planetary magnetic

field and heliocentric distance responds to strong solar activity. The combination of phenomena observed at Mars (e.g., transient flare heating and added ionization of neutrals, enhanced atmospheric ion pickup followed by precipitation or escape, SEP energy deposition-related atmospheric emissions) reveal both Earth-like and distinctly Martian responses during space weather storms. In addition, these observations reinforce the idea that space weather events have had impacts throughout the history of Mars and more broadly the solar system that cannot be ignored in the big-picture reconstructions of their evolution.

Acknowledgments. The MAVEN mission has been made possible through NASA sponsorship and the dedicated efforts of NASA Goddard Space Flight Center, LASP, Lockheed Martin, and the MAVEN Technical and Science Teams. The interpretation of the MAVEN observations described here benefitted from the earlier observations and analyses of space weather events on MEX which provided some examples of events from the more active preceding solar cycle.

The MAVEN and MSL data shown are publicly available at the NASA Planetary Data System website (http://ppi.pds.nasa.gov). The MEX ASPERA-3 data is available at the ESA Planetary Science Archive. The GOES-13 data is available at the NOAA National Centers for Environmental Information website (https://www.ngdc.noaa.gov/). The WSA-Enlil simulation results were provided by the NASA/GSFC Community Coordinated Modeling Center through their public Runs on Request system (http://ccmc.gsfc.nasa.gov). We also acknowledge using solar observations from

SOHO/LASCO, SDO/AIA, STA/EUVI and STA/SECCHI, and in situ measurements from STA/HET.

We would like to thank E. Thiemann, A. Rahmati, R. Lillis, P. Dunn, B. Ehresmann, J. Gruesbeck, P. Chamberlin, S. Xu, R. Ramstad, T. Hara, J. McFadden, C. Fowler, L. Andersson, J. Espley, A. Poppe, S. Curry, M. Elrod., S. Jain and N. Schneider for their helpful insights and discussions.

Notes

1. WSA-Enlil-cone event simulation made by special request through the NASA Community Coordinated Modeling Center; run name 'Leila_Mays_120817_SH_9'.

2. The start and end times are based on the full-width, half maximum values.

3. See the SOHO Halo CME alert at https://umbra.nascom.nasa.gov/lasco/observations/halo/2017/170910/

References

Arge, C.N., Luhmann, J.G., Odstrcil, D., Schrijver, C.J., Li, Y.: 2004, Stream structure and coronal sources of the solar wind during the May 12th, 1997 CME, *J. Atm Solar Terr. Phys.*, **66**, 1295–1309.

Aschwanden, M.J.: 1994, Irradiance observations of the 1–8 A solar soft X–ray flux from GOES, *Solar Phys.* **152**, 53–59.

Bain, H.M., M.L. Mays, J.G. Luhmann, Y. Li, L.K. Jian, D. Odstrcil, 2016: Shock connectivity in the August 405 2010 and July 2012 solar energetic particle events inferred from observations and ENLIL modeling, *Ap. J.*, 825, doi:10.3847/0004-637X/825/1/1.

Bornmann, P. L., Speich, D., Hirman, J., Matheson, L., Grubb, R., Garcia, H. A., Viereck, R.: 1996, GOES X-ray sensor and its use in predicting solar-terrestrial disturbances, In: SPIE 1996 International Symposium on Optical Science, Engineering, and Instrumentation, International Society for Optics and Photonics, 291-298.

Brain, D. A., J. S. Halekas, L. M. Peticolas, R. P. Lin, J. G. Luhmann, D. L. Mitchell, G. T. Delory, S. W. Bougher, M. H. Acuna, H. Reme, 2006, On the origin of aurorae on Mars, *Geophys. Res. Lett.*, **33(1)**, 01201, doi:10.1029/2005GL024782.

Brain, D. A., McFadden, J. P., Halekas, J. S., Connerney, J. E. P., Bougher, S. W., Curry, S., Dong, C. F., Dong, Y., Eparvier, F., Fang, X., Fortier, K., Hara, T., Harada, Y., Jakosky, B. M., Lillis, R. J., Livi, R., Luhmann, J. G., Ma, Y., Modolo, R., Seki, K.: 2015, The spatial distribution of planetary ion fluxes near Mars observed by MAVEN, *Geophys. Res. Lett.*, **41(21)**, 9142–9148, doi:10.1002/2015GL065293.

Brueckner, G.E., Howard, R.A., Koomen, M.J., Korendyke, C.M., Michels, D.J., Moses, J.D., Socker, D.G., Dere, K.P., Lamy, P.L., Llebaria, A., Bout, M.V., Schwenn, R., Simnett, G.M., Bedford, D.K., Eyles, C.J.: 1995, The Large Angle Spectroscopic Coronagraph (LASCO), *Solar Phys.* **162**, 357–402.

Capalbo, F. J.: 2010, Background Analysis for IMA Sensor on ASPERA Instrument, *IRF Technical Report* **54**, ISSN 0284-1738.

Cane, H.V.: 2000, Coronal mass ejections and Forbush decreases, *Space Sci. Rev.* **93**, 55–77.

Chamberlin, P. C., Woods, T. N., Didkovsky, L., Eparvier, F. G., Jones, A. R., Mason, J. P., Machol, J. L., Snow, M., Thiemann, E. M. B., Viereck, R. A., Woodraska, D. L.: 2018, Solar Ultraviolet Irradiance Observations of the Solar Flares During the Intense September 2017 Storm Period, *Space Weather*, submitted, 2018SW001866.

Connerney, J. E. P., J. Espley, P. Lawton, S. Murphy, J. Odom, R. Oliversen, D. Sheppard.: 2015, The MAVEN magnetic field investigation, *Space Sci. Rev.*, 1-35, doi: 10.1007/s11214-015-0169-4.

Crider, D.H., Espley, J., Brain, D.A., Mitchell, D.L., Connerney, J.E.P., Acuna, M.: 2005, Mars Global Surveyor observations of the Halloween 2003 solar superstorm's encounter

with Mars, *J. Geophys. Res.* **110**, A09S21, doi:10.1029/2001JA010881.

Dong, C., Ma, Y., Bougher, S. W., Toth, G., Nagy, A. F., Halekas, J. S., Dong, Y., Curry, S. M., Luhmann, J. G., Brain, D., Connerney, J. E. P., Espley, J., Mahaffy, P., Benna, M., McFadden, J. P., Mitchell, D. L., DiBraccio, G. A., Lillis, R. J., Jakosky, B. M., Grebowsky, J. M., 2015, Multifluid MHD study of the solar wind interaction with Mars' upper atmosphere during the 2015 March 8th ICME event, *Geophys. Res. Lett.*, **42(2)**, 9103–9112, doi:10.1002/2015GL065944.

Dubinin, E., Fraenz, M., Woch, J., Duru, F., Gurnett, D., Modolo, R., Barabash, S, Lundin, R.: 2009, Ionospheric storms on Mars: Impact of the corotating interaction region, *Geophys. Res. Lett*, **36**, doi:10.1029/2008GL036559.

Edberg, N. J. T., Nilsson H., Williams, A. O. , Lester, M., Milan, S. E., Cowley, S. W. H., Franz, M. , Barabash, S. Futaana, Y.: 2010, Pumping out the atmosphere of Mars through solar wind pressure pulses, *Geophys. Res. Lett.*, **370**, L03107, doi: 10.1029/2009GL041814.

Ehresmann, B., Hassler, D. M., Zeitlin, C. J., Guo, J., Wimmer-Schweingruber, R. F., Matthia, D., Lohf, H., Burmeister, S., Rafkin, S. C. R., Berger, T.; Reitz, G.: 2018, Energetic Particle Radiation Environment Observed by RAD on the Surface of Mars during the September 2017 Event, *Geophys. Res. Lett.*, **4511**, doi:10.1029/2018GL077801.

Elrod, M. K., Curry, S. M., Thiemann, E. M. B., Jain, S. K.: 2018, September 2017 Solar Flare Event: Rapid Heating of the Martian Neutral Exosphere from the X-class flare as observed by MAVEN, *Geophys. Res. Lett.*, in press, 2018GL077729.

Eparvier, F.G., Chamberlin, P.C., T.N. Woods, Thiemann, E.M.B.: 2015, The Solar Extreme Ultraviolet Monitor for MAVEN, *Space Science Reviews*, **195**, 293–301.

Espley, J., Cloutier, P.A., Crider, D.H., Brain, Acuna, M.: 2005, Low-frequency plasma oscillations at Mars during the October 2003 solar storm, *J. Geophys. Res.* **110**, A09S33.

Fallows, K., Withers, P., Gonzalez, G.: 2015, Response of the Mars ionosphere to solar flares: Analysis of MGS radio occultation data, *J. Geophys. Res.* **120**, 9805–9825.

Fang, X., Pawlowski, D., Ma, Y., Thiemann, E. M. B., Dong, C., Bougher, S., Eparvier, F., Brain, D., Lee, C. O., Dong, Y., Chamberlin, P., Benna, M., Elrod, M., Wang, W., Mahaffy, P., Jakosky, B. M.: 2018, Global simulation of Mars upper atmospheric effects of the 10 September 2017 solar flare, *Geophys. Res. Lett.*, submitted, 2018GL077829.

Fowler, C. M., L. Andersson, R. E. Ergun, M. Morooka, G. Delory, D. J. Andrews, R. J. Lillis, T. McEnulty, T. D. Weber, T. M. Chamandy, A. I. Eriksson, D. L. Mitchell, C. Mazelle, B. M. Jakosky: 2015: The first in situ electron temperature and density measurements of the Martian nightside ionosphere, *Geophys. Res. Lett.*, **42(21)**, 8854–8861, doi:10.1002/2015GL065267.

Futaana, Y., Barabash, S., Yamauchi, M., McKenna-Lawlor, S., Lundin, R., Luhmann, J.G., Brain, D., Carlsson, E., et al.: 2008: Mars Express and Venus Express multi-point observations of geoeffective solar flare events in December 2006, *Planetary and Space Science*, **56**, 873.

Girazian, Z., P. Mahaffy, R. J. Lillis, M. Benna, M. Elrod, C. M. Fowler, D. L. Mitchell: 2017, Ion Densities in the Nightside Ionosphere of Mars: Effects of Electron Impact Ionization, *Geophys. Res. Lett.*, **44**, 11,248–11,256, doi:10.1002/2017GL075431.

Gopalswamy, Yashiro, S., Liu, Y., Michalek, G., Vourlidas, A., Kaiser, M.L., Howard, R.A.: 2005, Coronal mass ejections and other extreme characteristics of the 2003 October-November solar eruptions, *J. Geophys. Res.*, **110**, A09S15, doi: 10.1029/2004JA010958.

Grotzinger, J. P., Crisp, J., Vasavada, A. R., Anderson, R. C., Baker, C. J., Barry, R., Blake, D. F., Conrad, P., Edgett, K., S., Ferdowski, B., Gellert, R., Gilbert, J. B., Golombek, M., Gomez-Elvira, J., Hassler, D. M., et al.: 2012, Mars Science Laboratory Mission and Science Investigation, *Space Sci. Rev.*, 170, 5–56.

Guo, J., Zeitlin, C., Wimmer-Schweingruber, R.F., McDole, T., Kuhl, P., Appel, J. C., Matthia, D., Krauss, J., Kohler, J.: 2018a, A generalized approach to model the spectra and radiation dose rate of solar particle events on the surface of Mars, *Astron. J.*, **155(49)**, doi:110.3847/1538-3881/aaa085 .

Guo, J., Lillis, R., Wimmer-Schweingruber, R. F., Zeitlin, C., Simonson, P., Rahmati, A., Posner, A., Papaioannou, A., Lundt, N., Lee, C. O., Larson, D., Halekas, J., Hassler, D. M., Ehresmann, B., Dunn, P., Bottcher, S.: 2018b, Measurements of Forbush decreases at Mars: both by MSL on ground and by MAVEN in orbit, *Astron. and Astrophys.*, **611(A79)**, doi:10.1051/0004-6361/201732087 .

Guo, J., Dumbovic, M., Wimmer-Schweingruber, R., F., Temmer, M., Lohf, H., Wang, Y., Veronig, A., Hassler, D. M., Mays, L. M., Zeitlin, C., Ehresmann, B., Witasse, O., von Forstner, J. L., F., Heber, B., Holmstrom, M., Posner, A.: 2018c, Modeling the evolution and propagation of the 2017 September 9th and 10th CMEs and SEPs arriving at Mars constrained by remote-sensing and in-situ measurement, *Space Weather*, accepted,

2018SW001973-T.

Gurnett, D. A., Kirchner, D. L., Huff, R. L., Morgan, D. D., Persoon, A. M., Averkamp, T. F., Duru, F., Nielsen, E., Safaeinili, A., Plaut, J. J., Picardi, G.: 2005, Radar soundings of the ionosphere of Mars, *Science*, **310(5756)**, 1929–1933, doi:10.1126/science.1121868

Gurnett, D., R. Huff, D. Morgan, A. Persoon, T. Averkamp, D. Kirchner, F. Duru, F. Akalin, A. Kopf, E. Nielsen, A. Safaeinili, J. Plaut, and G. Picardi: 2008, An overview of radar soundings of the martian ionosphere from the Mars Express spacecraft, *Adv. Space Res.*, **41(9)**, 1335–1346, doi:10.1016/j.asr.2007.01.062.

Halekas, J. S., E. R. Taylor, G. Dalton, G. Johnson, D. W. Curtis, J. P. McFadden, D. L. Mitchell, R. P. Lin, B. M. Jakosky: 2015, The Solar Wind Ion Analyzer for MAVEN, *Space Sci. Rev.*, **195**, 125–151.

Halekas, J. S., S. Ruhunusiri, Y. Harada, G. Collinson, , D. L. Mitchell, C. Mazelle, J. P. McFadden, J.E.P. Connerney, J.R. Espley, F. Eparvier, J.G. Luhmann, B. M. Jakosky: 2017, Structure, Dynamics, and Seasonal Variability of the Mars-Solar Wind Interaction: MAVEN Solar Wind Ion Analyzer Inflight Performances and Science Results, *J. Geophys. Res.*, **122**, 547–578.

Harada, Y., Gurnett, D. A., Kopf, A. J., et al.: 2018, MARSIS observations of the Martian nightside ionosphere during the September 2017 solar event, *Geophys. Res. Lett.*, in press, doi:10.1002/2018GL077622.

Harnett, E. M., and R. M. Winglee, 2006, Three-dimensional multifluid simulations of ionospheric loss at Mars from nominal solar wind conditions to magnetic cloud events, *J. Geophys. Res.*, **111(A)**, 09213, doi:10.1029/2006JA011724.

Hassler, D.M., Zeitlin, C., Wimmer-Schweingruber, R. F., Bottcher, S., Martin, C., Andrews, J., Bohm, E., Brinza, D. E., Bullock, M. A., Burmeister, S., Ehresmann, B., et al.: 2012, The Radiation Assessment Detector (RAD) Investigation, *Space Sci. Rev.*, **170**, 503-558, doi:10.1007/s11214-012-9913-1

Hassler, D. M., Zeitlin, C., Wimmer-Schweingruber, R. F., Ehresmann, B., Rafkin, S., Eigenbrode, J. L., Brinza, D. E., Weigle, G., Bottcher, S., Bohm, E., et al.: 2014: Mars' surface radiation environment measured with the Mars Science Laboratory's Curiosity Rover, *Science*, **343**, doi:10.1126/science.1244797.

Jain, S., Deighan, J., Schneider, N. M., et al.: 2018, Response of Martian thermosphere to the X8.2 solar flare of 10 September 2017 as seen by MAVEN/IUVS, *Geophys. Res. Lett.*, in press, doi:10.1029/2018GL077731.

Jakosky, B.M., et al.: 2015a, The Mars Atmosphere and Volatile Evolution (MAVEN) Mission, *Space Sci. Rev.*, doi:10.1007/s11214-015-0139-x.

Jakosky, B.M., et al.: 2015b, MAVEN observations of the response of Mars to an interplanetary coronal mass ejection from the Sun, *Science*, **350**, doi:10.1126/science.aad0210.

Kaiser, M.: 2005, The STEREO mission: an overview, *Adv. Space Res.*, **36**, 1483–1488.

Lario, D., Kwon, R. -Y., Riley, P., Raouafi, N. E.: 2017, On the link between the release of solar energetic particles measured at widespread heliolongitudes and the properties of the associated coronal shocks, *Astrophys. J.*, **847**, 103(22pp).

Larson, D.E. R.J. Lillis, Lee, C.O., K. Hatch, M. Robinson, D. Glaser, J. Chen, D.W. Curtis, C. Tiu, R.P. Lin, J.G. Luhmann, B.M. Jakosky: 2015, The MAVEN Solar Energetic Particle Investigation, *Space Sci. Rev.*, **195**, 153–172.

Lee *et al.*2013(@)(@)leeetal13 Lee, C.O., Arge, C.N., Odstrcil, D., Millward, G., Pizzo, V., Quinn, J.M., Henney, C.J.: 2013, Ensemble Modeling of CME Propagation, *Solar Phys.*, **285**, 349–368, doi:10.1029/2011SW000748.

Lee *et al.*2015(@)(@)leeetal15 Lee, C.O., Arge, C.N., Odstrcil, D., Millward, G., Pizzo, V., Lugaz, N.: 2015, Ensemble Modeling of Successive Halo CMEs: A Case Study, *Solar Phys.*, **290**, 1207–1229, doi:10.1007/s11207-015-0667-2.

Lee *et al.*2017(@)(@)leeetal17 Lee, C. O., Hara, T., Halekas, J. S., Thiemann, E., Chamberlin, P., Eparvier, F., Lillis, R. J., Larson, D. E., Dunn, P. A., Espley, J. R., Gruesbeck, J., Curry, S. M., Luhmann, J. G., Jakosky, B. M.: 2017: MAVEN observations of the solar cycle 24 space weather conditions at Mars, *J. Geophys. Res.*, **122**, doi: 10.1002/2016JA023495.

Lee, Y., Dong, C., Pawlowski, D.. et al.: 2018, Effects of a Solar Flare on the Martian 1 Hot O Corona and Photochemical Escape, *Geophys. Res. Lett.*, accepted, 2018GL077732.

Lemen, J. R., et al.: 2012, The Atmospheric Imaging Assembly (AIA) on the Solar Dynamics Observatory (SDO), *Solar Phys.*, doi:10.1007/s11207-011-9776-8.

Lillis, R. J., C. O. Lee, D. E. Larson, J. G. Luhmann, J. S. Halekas, J. E. P. Connerney, B. M. Jakosky: 2017, Photochemical escape of oxygen from Mars: First results from MAVEN in situ data, *J. Geophys. Res.*, **122(3)**, 3815–3836, doi:10.1002/2016JA023525.

Lollo, A., Withers, P., Fallows, K., Girazian, Z., Matta, M., Chamberlin, P. C.: 2012, Numerical simulations of the ionosphere of Mars during a solar flare, *J. Geophys. Res.*, **117(A5314)**, doi:10.1029/2011JA017399.

Luhmann, J.G., Mays, M. L., Odstrcil, D., Li, Y., Bain, H., Lee, C.O., Galvin, A. G., Mewaldt, R. A., Cohen, C. M. S., Leske, R. A., Larson, D., Futaana, Y.: 2017, Modeling Solar Energetic Particle Events Using ENLIL Heliospheric Simulations, *Space Weather*, **15**, 934–954, doi:10.1002/2017SW001617.

Luhmann, J. G., Mays, M. L., Li, Y., Lee, C. O., Bain, H., Odstrcil, D., Mewaldt, R. A., Cohen, C. M. S., Larson, D., Petrie, G.: 2018, Shock connectivity and the late cycle 24 solar energetic particle events in July and September 2017, *Space Weather*, in press, doi:10.1029/2018SW001860

Ma, Y. J., Nagy, A. F., 2007, Ion escape fluxes from Mars, *Geophys. Res. Lett.*, **34(8)**, 08201, doi:10.1029/2006GL029208.

Ma, Y., Fang, X., Halekas, J. S., et al.: 2018, The Impact and Solar wind Proxy of the 2017 September ICME Event at Mars, *Geophys. Res. Lett.*, in press, 2018GL077707.

Mahaffy, P. R., et al.: 2015, The Neutral Gas and Ion Mass Spectrometer on the Mars Atmosphere and Volatile Evolution Mission, *Space Sci. Rev.*, **195**, 49–73, doi: 10.1007/s11214-014-0091-1.

Mays, M.L., Taktakishvili, A., Pulkkinen, A., MacNeice, P. J., Rasttter, L., Odstrcil, D., Jian, L. K., Richardson, I. G., LaSota, J. A., Zheng, Y., Kuznetsova, M. M.: 2015, Ensemble modeling of CMEs using the WSA-ENLIL+Cone model, *Sol. Phys.*, **290**, 1775–1814, doi:10.1007/s11207-015-0692-1

Mayyasi, M., Bhattacharyya, D., Clarke, J., Benna, M., Mahaffy, P., Thiemann, E. M. B., Lee, C. O., Deighan, J., Jain, S., Chaffin, M., Crismani, M., McClintock, W., Stewart, I., Holsclaw, G., Stiepan, A., Montmessin, F., Schneider, N., Jakosky, B.: 2018, Significant

Space Weather Impact on the Escape of Hydrogen from Mars, *Geophys. Res. Lett.*, in press, 2018GL077727.

Mendillo, M., Klobuchar, J. A., Fritz, R. B., Da Rosa, A. V., Kersley, L., Yeh, K. C., et al.: 1974, Behavior of the ionospheric F region during the great solar flare of August 7, 1972, *J. Geophys. Res.*, **79(4)**, 665–672.

Millward *et al.*2013(@)(@)millwardetal13 Millward, G., Biesecker, D., Pizzo, V., de Koning, C.A.: 2013, An operational software tool for analysis of coronagraph images: Determining CME parameters for input into the WSA-Enlil heliospheric model, *Space Weather*, **11**, 57–68, doi:10.1002/swe.20024.

Norman *et al.*2014(@)(@)normanetal14 Norman, R. B., Gronoff, G., Mertens, C. J.: 2014, Influence of dust loading on atmospheric ionizing radiation on Mars, *J. Geophys. Res.*, **119**, 452–461, doi:10.1002/2013JA019351.

Odstrcil, D.: 2003, Modeling 3D solar wind structure, *Adv. Space Res.*, **32**, 497–506.

Pesnell, W. D., B. J. Thompson, and P. C. Chamberlin: 2012, The Solar Dynamics Observatory (SDO), *Solar Phys.*, doi:10.1007/s11207-011-9841-3.

Ramstad, R., Barabash, S., Futaana, Y., Nilsson, H., Wang, X.-D., Holmstrom, M. 2015, The Martian atmospheric ion escape rate dependence on solar wind and solar EUV conditions I: Seven years of Mars Express observations, *J. Geophys. Res.*, **120(7)**, 1298–1309.

Ramstad, R., S. Barabash, Y. Futaana, M. Yamauchi, H. Nilsson, and M. Holmstrom, 2017, Mars Under Primordial Solar Wind Conditions: Mars Express Observations of the Strongest CME Detected at Mars Under Solar Cycle #24 and its Impact on Atmospheric

Ion Escape, *Geophys. Res. Lett.*, **44(2)**, doi::10.1002/2017GL075446.

Ramstad, R., Holmstrom, M., Futaana, Y., Lee, C. O., Rahmati, A., Dunn, P., Lillis, R. J., Larson, D.: 2018, The September 2017 SEP event in context with the current solar cycle: Mars Express ASPERA-3/IMA and MAVEN/SEP observations, *Geophys. Res. Lett.*, in press, doi:10.1029/2018GL077842.

Ribas, I., E. F. Guinan, M. Gudel, and M. Audard, 2005, Evolution of the Solar Activity over Time and Effects on Planetary Atmospheres. I. High-Energy Irradiances (1-1700$\AA$), *Astrophys. J.*, **622(1)**, 680–694, doi::10.1086/427977.

Romanelli, N., Modolo, R., LeBlanc, F., Chaufray, J-Y., Martinez, A., Ma, Y., Lee, C. O., Luhmann, J. G., Halekas, J., Brain, D., DiBraccio, G., Espley, J., McFadden, J., Jakosky, B., Holmstrom, M.: 2018, Responses of the Martian magnetosphere to an interplanetary coronal mass ejection: MAVEN observations and LatHyS results, *Geophys. Res. Lett.*, in press, 2018GL077714.

Saunders et al.2014(@)(@)saundersetal04 Saunders, R. S., Arvidson, R. E., Badhwar, G. D., Boynton, W. V., Christensen, P., Cucinotta, F. A., Gibbs, R. G., Kloss, Jr. C., Landano, M. R., Mase, R. A., Meyer, M., Pace, G., Plaut, J. J., Sidney, W., McSmith, G. W., Spencer, D. A., Thompson, T. W. and Zeitlin, C. J.: 2004, 2001 Mars Odyssey Mission Summary, *Space Sci. Rev.*, (110), 1–36.

Schneider, N., Deighan, J. I., Jain, S. K., Stiepen, A., Evans, J. S., Stewart, A. I. F., Larson, D., Mitchell, D. L., Lee, C. O., Lillis, R., Brain, D., Stevens, M. H., et al.: 2015, The discovery of diffuse aurora on Mars, *Science*, **350**, doi:10.1126/science.aad0313.

Schneider, N., Jain, S. K., Deighan, J. I., Nasr, C. R., Brain, D. A., Larson, D., Lillis, R., Rahmati, A., Halekas, J. S., Lee, C. O., Chaffin, M. S., et al.: 2018, Global Aurora on Mars during the September 2017 Space Weather Event, *Geophys. Res. Lett.*, in press, 2018GL077772.

Thiemann, E. M. B., Eparvier, F. G., Andersson, L. A., Fowler, C. M., Peterson, W. K., Mahaffy, P. R., Deighan, J. I.: 2015, Neutral density response to solar flares at Mars, *Geophys. Res. Lett.*, **42(21)**, 8986–8992.

Thiemann, E. M. B., Andersson, L. A., Lillis, R., Withers, P., Xu, S., Elrod, M., Jain, S., Pilinski, M. D., Pawlowski, D., Chamberlin, P. C., Eparvier, F. G., Benna, M., Fowler, C., Curry, S., Peterson, W. K.: 2018, The Mars Upper Ionosphere Response to the X8.2 Solar Flare of 10 September 2017, *Geophys. Res. Lett.*, in press, 2018GL077730.

Trotignon, J. G., Mazelle, C., Bertucci, C., Acuna, M. H., 2006, Martian shock and magnetic pile-up boundary positions and shapes determined from the Phobos 2 and Mars Global Surveyor data sets, *Planetary and Space Science*, **54(4)**, 357–369, doi: 10.1016/j.pss.2006.01.003.

von Rosenvinge, T. T., Reames, D. V., Baker, R., Hawk, J., Nolan, J. T., Ryan, L., Shuman, S., ...Wiedenbeck, M.E., 2008, The High Energy Telescope for STEREO, *Space Sci. Rev.*, **136**, 391–335, doi:10.1007/s11214-007-9300-5.

Witasse, O., Snchez-Cano, B., Mays, M. L., Kajdic, P., Opgenoorth, H., Elliott, H. A., Richardson, I. G., Zouganelis, I., Zender, J., Wimmer-Schweingruber, R. F., Turc, L., et al.: 2017, Interplanetary coronal mass ejection observed at STEREO-A, Mars, comet 67P/Churyumov-Gerasimenko, Saturn, and New Horizons en route to Pluto:

Comparison of its Forbush decreases at 1.4, 3.1, and 9.9 AU, *J. Geophys. Res.*, **122(8)**, 7865-7890, doi:10.1002/2017JA023884.

Withers, P., 2011, Attenuation of radio signals by the ionosphere of Mars: Theoretical development and application to MARSIS observations, *Radio Science*, **46(2)**, doi: 10.1029/2010RS004450.

Wood, B. E., H. R. Mller, G. P. Zank, J. L. Linsky, and S. Redfield, 2005, New Mass-Loss Measurements from Astrospheric Lyα Absorption, *Astrophys. J.*, **628(2)**, L143–L146, doi:10.1086/432716.

Xu, S., Fang, X., Mitchell, D. L., Ma, Y., Luhmann, J. G., DiBraccio, G. A., Weber, T., Brain, D., Mazelle, C., Curry, S. M., Lee, C. O.: 2018a, Investigation of Martian magnetic topology response to 2017 September ICME, *Geophys. Res. Lett.*, in press, 2018GL077708.

Xu, S., Thiemann, E., Mitchell, D. L., Eparvier, F., Pawlowski, D., Benna, M., Andersson, L., Liemohn, M. W., Bougher, S., Mazelle, C.: 2018b, Observations and modeling of low-altitude ionospheric responses to 2017 September solar flare at Mars *Geophys. Res. Lett.*, in press, 2018GL077709.

Zeitlin, C.J., Hassler, D. M., Cucinotta, F. A., Ehresmann, B., Wimmer-Schweingruber, R. F., Brinza, D. E., Kang, S., Weigle, G., Bottcher, S., Bhm, E., Burmeister, S., Guo, J., Khler, J., Martin, C., Posner, A., Rafkin, S., Reitz, G.: 2013, Measurements of Energetic Particle Radiation in Transit to Mars on the Mars Science Laboratory, *Science*, **340**, 1080–1084, doi:10.1126/science.1235989.

Zeitlin, C., Hassler, D. M., Guo, J., Ehresmann, B., Wimmer-Schweingruber, R. F., Rafkin, S. C. R., Freiherr von Forstner, J. L., Lohf, H., Berger, T., Matthiae, D., Reitz, G.: 2018, Analysis of the radiation hazard observed by RAD on the surface of Mars during the September 2017 solar particle event, *Geophys. Res. Lett.*, *45(12)*, 5845–5851, doi:10.1029/2018GL077760.

Table 1. Timeline of Events at Mars during the September 2017 Solar Events Period

Date	Time (UT)	Event Description	Mission/ Instrument	Related References
10 Sept	15:40:30	Start of X8.2 flare in 0-7nm solar irradiance	MAVEN/EUVM	*Chamberlin et al.* [2018]
	15:54:00	Detection of solar hard x-rays from X8.2 flare	MAVEN/SEP	this study
	15:54:34	CME eruption	SDO/AIA	*Guo et al.* [2018b]
	16:00:00	First appearance of CME in coronagraph FOV	SOHO/LASCO C2	
	16:02:00	Peak of X8.2 flare in Lyman-α	MAVEN/EUVM	*Chamberlin et al.* [2018]
	16:03:40	80% enhancement in ionizing EUV irradiance	MAVEN/EUVM	*Thiemann et al.* [2018]
	16:11:30	Peak of X8.2 in 0-7 nm solar irradiance	MAVEN/EUVM	*Chamberlin et al.* [2018]
	17:30:41[a]	Expansion of neutral atmosphere from flare heating	MAVEN/NGIMS	*Elrod et al.* [2018]
	17:35:56[a]	70 K increase in thermospheric temperature	MAVEN/IUVS	*Jain et al.* [2018]
	19:20:00	Arrival of 20-200 keV SEP electrons	MAVEN/SEP	this study
	19:50:00	Rise in surface radiation above background level and arrival of >275 MeV/nuc ion	MSL/RAD	*Zeitlin et al.* [2018] *Guo et al.* [2018b] *Ehresmann et al.* [2018]
	22:00:00	Arrival of 80-220 MeV SEP protons	MAVEN/SEP	this study
		Arrival of 15-100 MeV SEP protons	MAVEN/SEP	this study
		Rise in penetrating background counts	MAVEN/SWEA	this study
	23:30:00	Impact by an SIR	MAVEN/SWIA &MAG MEX/ASPERA-3	this study
	23:38:04[b]	Rise in penetrating background counts rate	MEX/ASPERA-3	*Ramstad et al.* [2018]
11 Sept	2:34:00	IMF draping down to 200 km due to SIR	MAVEN/SWEA, MAG	*Xu et al.* [2018a]
	6:30:00	Peak in proton fluxes at the surface	MSL/RAD	*Ehresmann et al.* [2018]
		Peak in surface dose rate		*Zeitlin et al.* [2018]
	18:52:30	Peak in 80-220 MeV SEP protons	MAVEN/SEP	this study
12 Sept	17:57:30	Peak in 15-100 MeV SEP protons	MAVEN/SEP	this study
13 Sept	2:30:00	Peak emission of diffuse aurora	MAVEN/IUVS	*Schneider et al.* [2018]
	2:52:13	ESP enhancement due to ICME shock arrival	MAVEN/SWEA, SEP	this study
		Onset of Forbush Decrease	MSL/RAD	*Guo et al.* [2018b]
		IMF draping down to 300 km due to ICME	MAVEN/SWEA, MAG	*Xu et al.* [2018a]
	5:40:00	SEP bite-out from magnetic cloud	MAVEN/SWEA, SEP	this study

[a] Closest time available from MAVEN periapsis measurements. [b] Time after observational data gap.

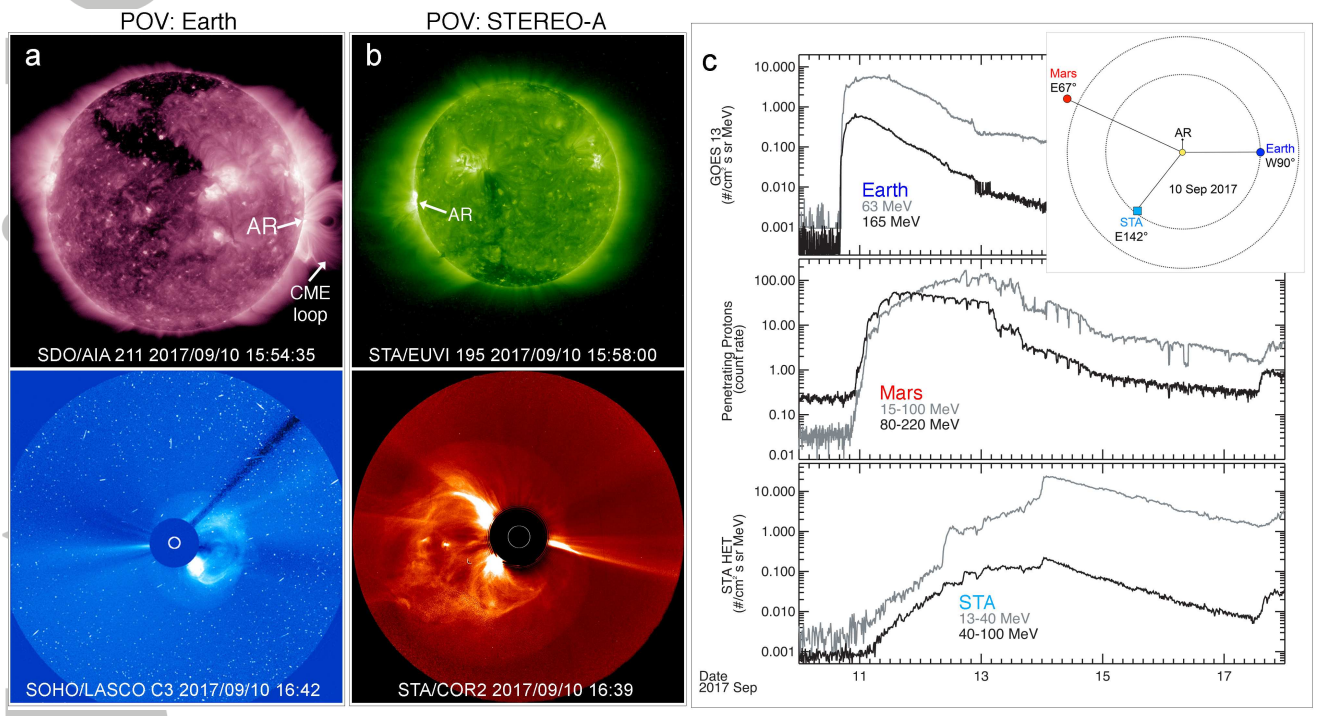

Figure 1. (a) Top panel shows the CME eruption site near AR2673 on the solar disk by SDO/AIA. Bottom panel shows the CME structure at 16:24 UT by SOHO/LASCO C3. (b) Top panel shows the eruption site from STA/EUVI. Bottom panel shows CME structure at 16:24 UT by STA/COR2. (c) Higher energy (dark gray) and lower energy (light gray) SEP proton observations by GOES-13 at Earth (top panel), MAVEN/SEP at Mars (middle panel), and STA/HET (bottom panel). The inset shows the Earth, Mars, and STA heliolongitude locations with respect to the AR2673 location on the Sun, as labeled.

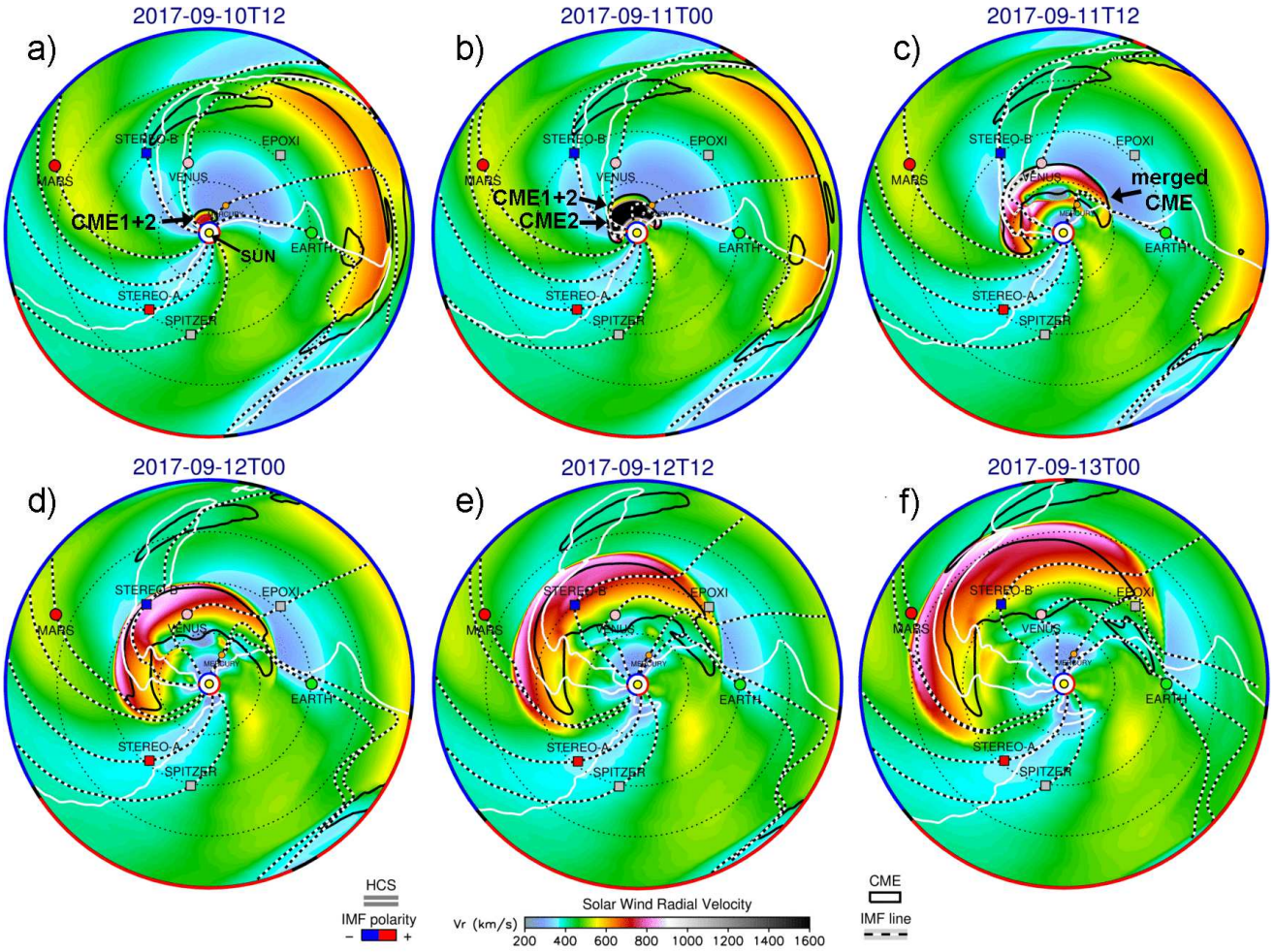

Figure 2. WSA-Enlil simulation snapshots showing the eruption and evolution of the 10 Sept 2017 CME structure, from 21.5 $R_{\odot}$ to Mars (red circle). (a) Two CMEs that erupted on 9 Sept 2017 CME appear in the simulation frame as a merged structure (CME1+2). (b) The 10 Sept 2017 CME (CME3) approaches CME1+2 from behind. (c–f) CME1+2 and CME3 propagate toward Mars as a merged structure. The colors shown are the modeled radial solar wind speeds in the ecliptic plane.

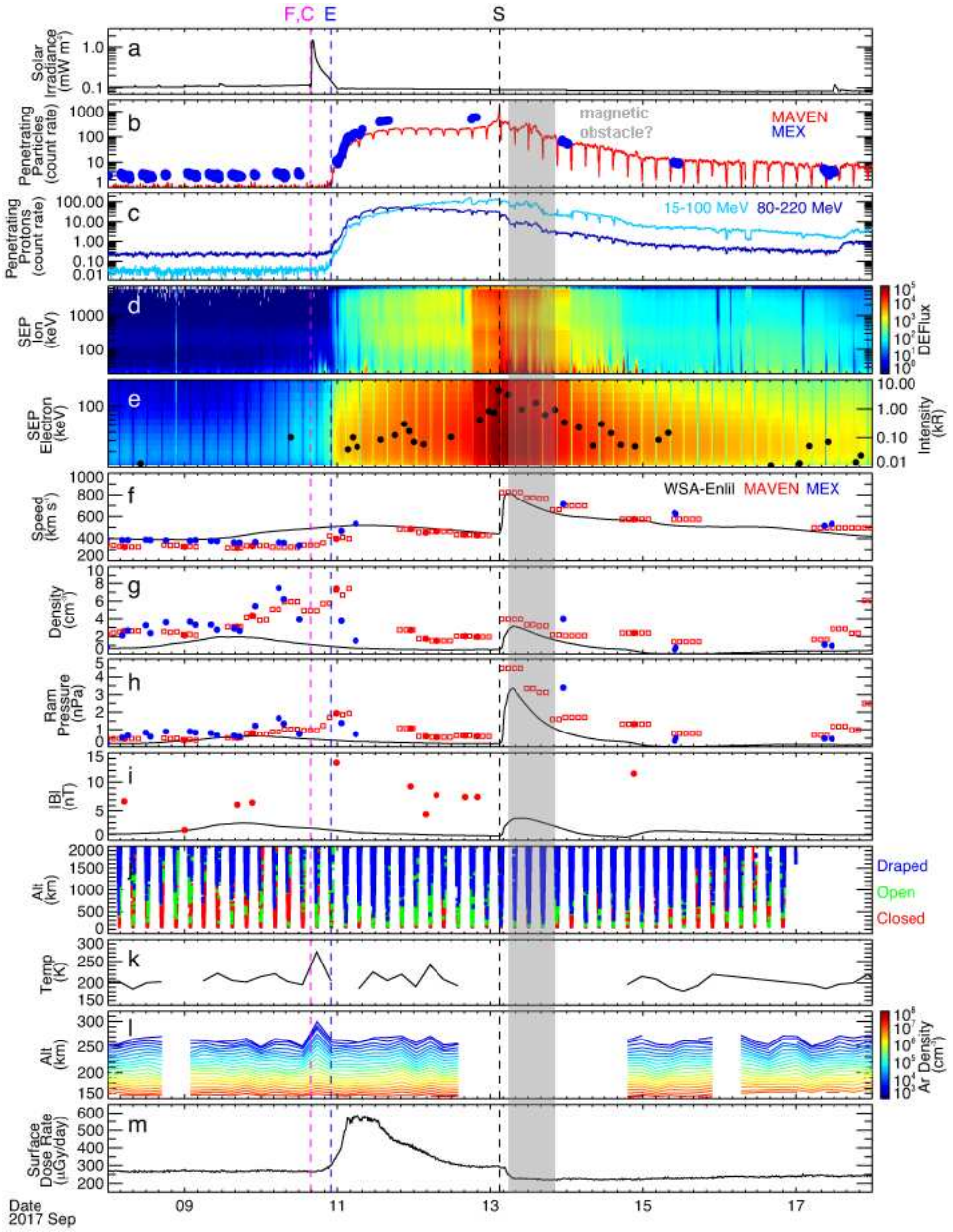

Figure 3. (a) MAVEN/EUVM solar irradiance in the 0.1-7 nm wavelength. (b) Penetrating background counts from MAVEN/SWEA (red) and MEX/ASPERA-3 IMA (blue). (c) 15-100 MeV (light blue) and 80-200 MeV (blue) SEP protons from MAVEN/SEP-FTO. (d–e) Differential energy fluxes of the MAVEN/SEP 20 keV to 6 MeV protons and 20 keV to 200 keV electrons. Overplotted are the IUVS auroral emission in kiloRayleighs (black circles). (f–i) Upstream solar wind speed, density, dynamic pressure, and IMF magnitude from MAVEN/SWIA and MAG (red filled circles), MEX/ASPERA-3 IMA (blue filled circles) and WSA-Enlil model (black line). Proxy solar wind values estimated from the MAVEN/SWIA penetrating proton measurements are also shown (red open squares). (j) Closed (red), open (green), and draped (blue) magnetic field topology for a given altitude. (k) Inferred thermospheric temperatures. (l) Color contours of Argon densities at a given height. (m) MSL/RAD surface radiation dose rate. Vertical lines mark the start of the flare (F), CME (C), SEP arrival (E), and ICME shock arrival (S). The vertical gray bar marks the 'bite-out' features seen in (b–c) by ICME magnetic cloud (MC) passage.

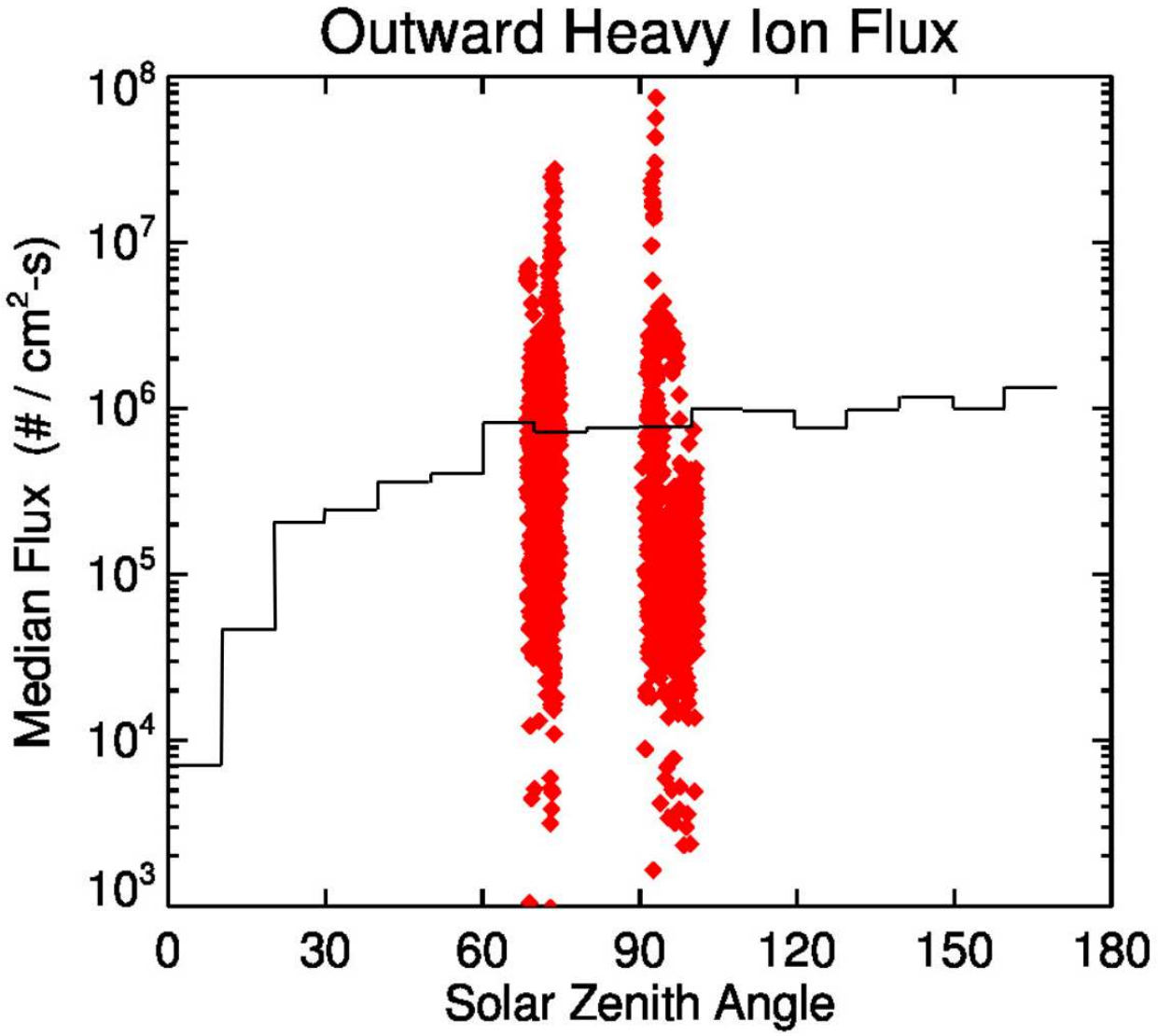

Figure 4. Orbit geometries for MAVEN (green track) and MEX (orange track), color-coded by time. (a) Orbital paths are shown in cylindrical coordinates. The inner line is the average location of the magnetic pileup boundary while the outer line is the average location of the bow shock [*Trotignon et al.*, 2006]. (b) Orbits projected onto the radial component of crustal magnetic field at 400 km as determined by Connerney et al. (2002). The dayside and nightside (shaded region) are separated by the terminator (curved black line) at the time of periapsis. The + symbol marks the MAVEN periapsis location (∼150 km at 03:20:22 UT on 13 Sept 2017). (c) View of Mars from above the MAVEN periapsis location, with the two spacecraft trajectories, crustal fields and shaded night side.

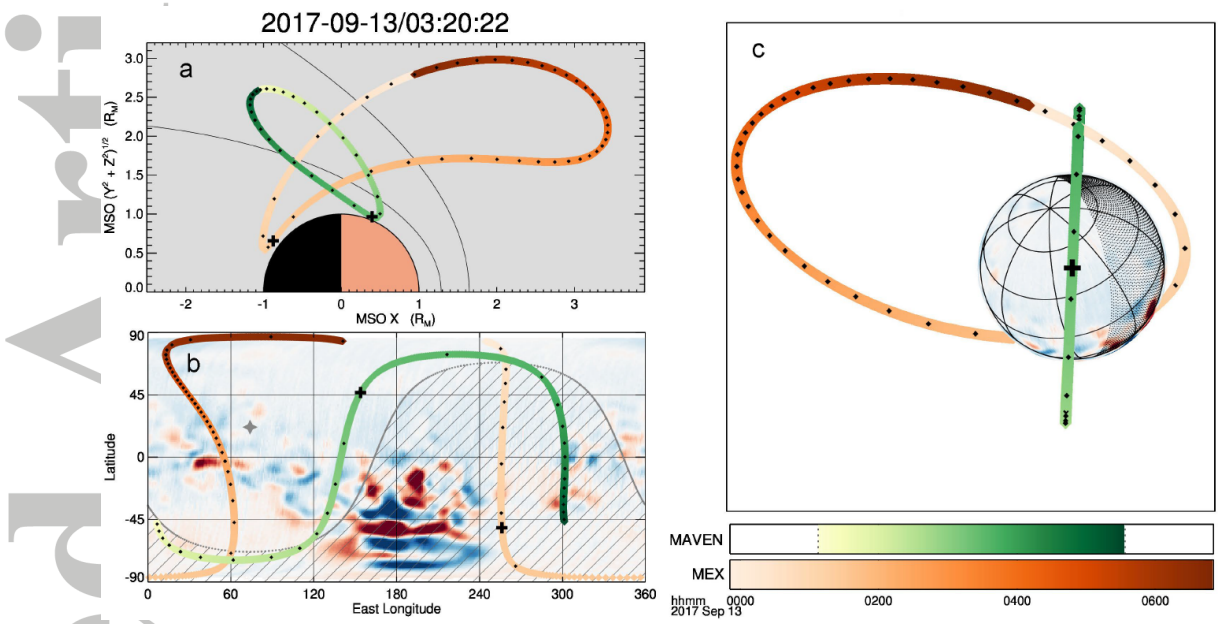

Figure 5. Comparison of outward-directed planetary heavy ion fluxes measured by MAVEN from 10 Sept 2017 through 18 Sept 2017 (red symbols) to the median outward directed fluxes measured by MAVEN from November 2014 through September 2016 (black line as a function of SZA). All observations were taken from a 1.25-1.45 R_M spherical shell around Mars.